A CFD-DEM Based Numerical Investigation of Debris Flow on Ballasted Railway Track

Yufeng Gong[1], and *Yu* Qian[1*]

[1]Department of Civil and Environmental Engineering, University of South Carolina, Columbia, South Carolina 29208, USA

Abstract Debris flow occurring in mountainous areas can cause issues to railway tracks. Debris flow may cause large track deformation and even track breakage and introduce server ballast fouling afterwards. After the flash of a debris flow, the fine particles can be retained in the ballast layer and significantly reduce track drainage, leading to lower bearing capacity and a higher risk of track lateral stability problems. Moreover, these solid particles may deposit on the railway surface and endanger the train directly. Unfortunately, those debris flow introduced track issues have not been thoroughly investigated. This study presents a numerical investigation of the impact of the debris flow on the railway track. Various factors governing the debris flow are considered, including particle size and solid fraction. Besides, those factors affecting the ballast are also discussed, such as fouling condition and initial void ratio. A coupled computational fluid dynamics and discrete element method (CFD-DEM) approach is developed to capture the interactions between particles/particles, water/air, and particles/fluid. The results from this study may help the railway to improve track resilience before the debris flow and to improve maintenance strategy after the debris flow flashing.

1 Introduction

The debris flow threads the safety of railway engineering in mountainous areas [1-4]. Not only the direct impact of the debris flow onto the train but also the impairing on the structure of the railway, especially the substructure. This may cause service disruption and even derailments and fatalities.

When fine particles in debris flow are detained by the ballast aggregates, they fill the voids and cause ballast fouling [5]. Fouled ballast often leads to excessive settlement, degraded track modulus, and poor drainage.

Traditionally, the finite element method (FEM) and computational fluid dynamics (CFD) are popular numerical methods to investigate the fouling effects on the ballast [6-10]. However, these methods use the porous media to represent granular materials and ignore the movement of fine particles within the ballast. For a better maintenance strategy, it is critical to understand how and where fines would initiate settlement and cumulate in the ballast under a certain driven force, like rainfall seepage, train-induced vibration, and debris flow flashing.

The coupled computational fluid dynamics and discrete element method (CFD-DEM) has recently been used widely in the geotechnical and geological areas [11-13]. With coupled CFD-DEM, the motion of particles can be captured, and the influence of particles on the fluid can also be simulated. This study employs an improved CFD-DEM model by including two different fluids, water and air. Hence the migration of fine particles in the ballast layer can be simulated without the assumption of a fully saturated track. Moreover, the quantified fine particle accumulation and water content distribution throughout the ballast layer can assist in decision-making for railway maintenance.

2 Methodology

2.1 Computational domain

The computational domain in this study contains a typical railway cross-section in North America [9,10,14,15]. For a newly constructed ballast layer, the size of aggregates ranges from 0.019 m to 0.051 m but is mostly uniformly graded. This study simplifies the complexity by assuming all the ballast aggregates share the same cubical shape having a side of 0.025 m. All these aggregates are subtracted from the computational domain and left with their outlines as a wall boundary. Totally, 1,292 aggregates are introduced and arranged in a staggered formation, forming a porous region with a porosity of 0.4, similar to the field condition.

Fig. 1 shows the sizes of the computational domain and the ballasted track. The thickness of the domain in the longitudinal direction is 0.025 m to save the
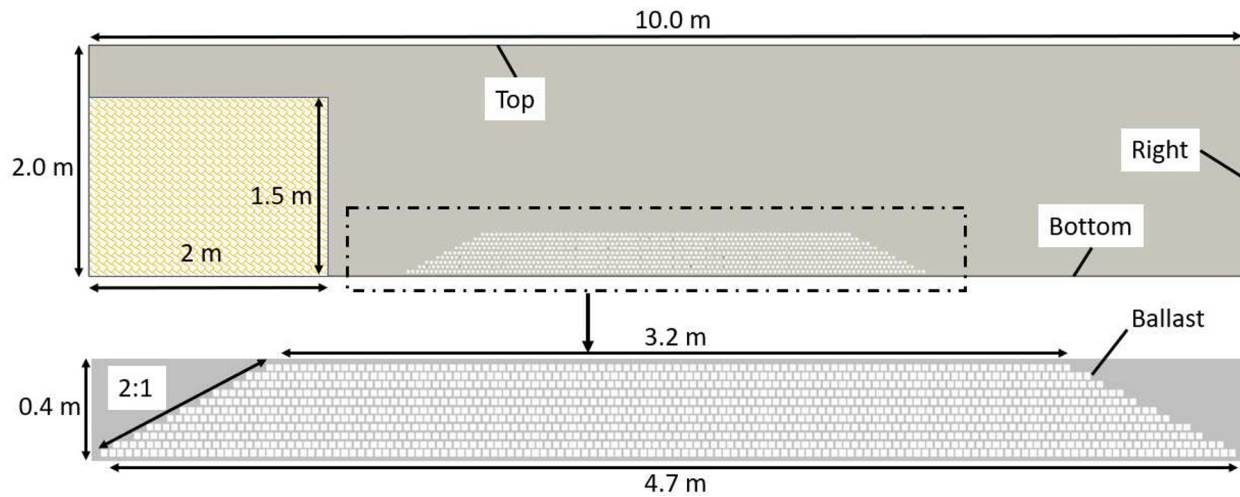

Fig. 1. Computational domain of fluid zone populated with the ballast

computational resource and to include one full ballast. The top, bottom, and ballast outlines are set to be wall boundaries. A vertical slope with size 1.5m x 2 m filled with backfillings is set to fail after saturation, then the debris flow forms and advances towards the railway ballast layer. The right is set to be pressure outlet. During the whole simulation, the solid particles from the debris flow are tracked and used to quantify the performance of the rail track.

2.2 Governing equations of the CFD-DEM method

The CFD-DEM method involves two different types of phases: the continuous phase-fluid and the discrete phase-solid. In this study, the continuous phase is composed of two different fluids: water and air, and its governing equations are formulated as follows:

$$\frac{\partial(\alpha_c\rho_c\mathbf{U}_c)}{\partial t} + \nabla\cdot(\alpha_c\rho_c\mathbf{U}_c\mathbf{U}_c) =$$
$$\nabla\cdot(\alpha_c\boldsymbol{\tau}) - \mathbf{g}\cdot\mathbf{h}\nabla\rho_c - \nabla p_{rgh} + \sigma\kappa\nabla\alpha_1 - \mathbf{F}_s \quad (1)$$

$$\frac{\partial\alpha_c}{\partial t} + \nabla\cdot(\alpha_c\mathbf{U}_c) = 0 \quad (2)$$

where α_c is the volume fraction of the continuous phase in every cell, ρ_c is the density of the fluid mixture, and $\mathbf{U}_c$ is the velocity of the continuous phase. On the right-hand side of **Eq. (1)**, $\boldsymbol{\tau}$ is the shear stress tensor, $\mathbf{g}$ is the gravitational acceleration vector, $\mathbf{h}$ is the coordinate vector, $p_{rgh} = p - \rho\mathbf{g}\cdot\mathbf{h}$ is the modified pressure, σ is the fluid surface tension coefficient, κ is the curvature at the water-air interface, α_1 is the volume fraction of the water in the continuous phase, and $\mathbf{F}_s$ is the cell-averaged solid-fluid interaction force. Moreover, α_2 is the volume fraction of the air in the continuous phase, correspondingly.

Besides, in order to increase the resolution of the volume fraction at the water-air interface, this modified volume of fluid (VOF) equation is employed:

$$\frac{\partial(\alpha_c\alpha_1)}{\partial t} + \nabla\cdot(\alpha_c\alpha_1\mathbf{U}_c) + \nabla\cdot\left(\alpha_c\alpha_1(1-\alpha_1)c|\mathbf{U}_c|\frac{\nabla\alpha_1}{|\nabla\alpha_1|}\right) = 0 \quad (3)$$

where c is a coefficient controlling the interface resolution.

For the discrete phase, Newton's second law of motion is used to formulate the equations for every single particle:

$$m_i\frac{d\mathbf{u}_i}{dt} = \Sigma_j\mathbf{F}_{ij}^c + m_i\mathbf{g} + \mathbf{f}_i^d + \mathbf{f}_i^{\nabla p} \quad (4)$$

$$I_i\frac{d\boldsymbol{\omega}_i}{dt} = \Sigma_j\mathbf{M}_{ij}^c \quad (5)$$

where m_i, I_i, $\mathbf{u}_i$, and $\boldsymbol{\omega}_i$ are a particle's mass, moment of inertia, velocity, and angular velocity. $\mathbf{F}_{ij}^c$ and $\mathbf{M}_{ij}^c$ are the contact force and contact moment within particles.

Two forces are considered in this research to account for the solid-fluid interaction force, the drag force $\mathbf{f}_i^d$ and the pressure gradient force $\mathbf{f}_i^{\nabla p}$. Ergun-Wen-Yu drag model is widely used and has the expression:

$$\mathbf{f}_i^d = \begin{cases} \frac{m_i}{\rho_i}\left[150\frac{(1-\alpha_c)\mu_c}{\alpha_c^2 d_i^2} + 1.75\frac{\rho_c|\mathbf{u}_i - \mathbf{U}_c|}{d_i}\right], \alpha_c < 0.8 \\ \frac{3}{4}\frac{m_i}{\rho_i}C_d\frac{\rho_c|u_i - U_c|}{\alpha_c^{2.65}d_i}, \quad \alpha_c \geq 0.8 \end{cases} \quad (6)$$

where m_i, ρ_i, and d_i are the mass, volume, and diameter of a particle, μ_c is the dynamic viscosity, and C_d is the drag coefficient. C_d depends on the value of the particle Reynolds number $Re = \alpha_c\rho_c d_i|\mathbf{u}_i - \mathbf{U}_c|/\mu_c$ and is determined by the equation [16]:

$$C_d = \begin{cases} 0.44, Re > 1000 \\ \frac{24}{Re}(1 + 0.15Re^{0.687}), Re \leq 1000 \end{cases} \quad (7)$$

The pressure gradient force is formulated as:

$$\mathbf{f}_i^{\nabla p} = -\frac{m_i}{\rho_i}\nabla p \quad (8)$$

Detailed parameters employed in modelling the debris flow are summarized in **Table 1**.

Table 1. Parameters used in the physical modelling

Items	Properties	Value

Particle	Density, kg/m³	2.65e3
	Young's modulus, GPa	70
	Poisson's ratio	0.3
	Restitution coefficient	0.7
	Rolling friction coefficient	0.15
Water	Density, kg/m³	1e3
	Viscosity, Pa·s	1e-06
Air	Density, kg/m³	1
	Viscosity, Pa·s	1.48e-05

The test matrix listed in **Table 2** is performed to study the influence of the debris flow on the ballasted track parametrically and quantitatively.

Table 2. Tests matrix

	Debris Flow		Ballasted Track	
No.	Diameter, m	Solid fraction	Fouling Profile	Void Ratio
1	4.75e-3	0.5	Clean	0.67
2	4.75e-3	0.3	Clean	0.67
3	4.75e-3	0.5	Moderately Fouled	0.67
4	4.75e-3	0.3	Moderately Fouled	0.67

3 Preliminary Discussion

According to the definition of fouling index [5], fouling index (FI) equals the summation of the accumulative passing of No.4 (4.75 mm) and No.200 (0.074 mm) sieves. Because it is assumed the ballast particles are cubic with the same size. Assuming that the density of these ballast stones is 2.7e3 kg/m³, the density of granite, the total mass of ballast is:

$$M_b = 1292 \times 2700 \times 0.0254^3 = 57.16 \text{ kg} \quad (9)$$

Since the particle diameter in the debris flow is no larger than the No.4 sieve, the flowing equation can be used to quantify the FI in the track after the debris flow flashing:

$$\text{FI} = \frac{M_r}{M_r + M_b} = \frac{N_r d_i^3}{N_r d_i^3 + 0.041} \quad (10)$$

where N_r is the number of solid particles retained with the track region.

Besides, the distribution of the retained solid particles changes as time evolves. To capture the spatial distribution of particles, the ballast domain is discretized into a mesh of size 60×6, as shown in **Fig. 2**. In each cell, a new index-local fouling occupancy (LFO) is defined to represent the number of particles in every cell:
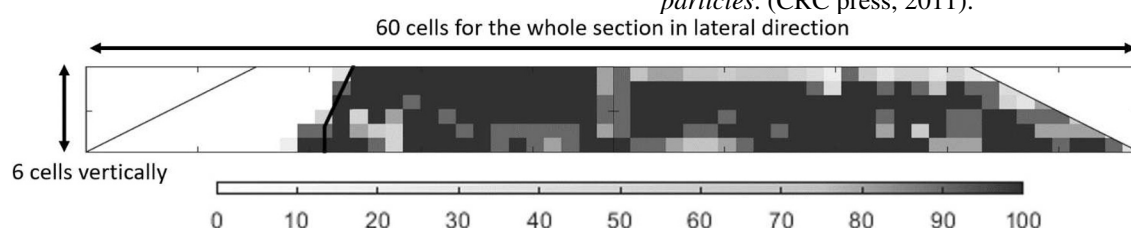
$$\text{LFO} = \frac{V_r^C}{\dfrac{4.7244 \times 0.381 \times 0.025}{30 \times 6}} \times 100\% \quad (11)$$

Also, with the new post-processing mesh, water content distribution can be quantified if any water is left within the ballast layer.

References

1. M. Pastor, J. A. F. Merodo, M. Quecedo, M. I. Herreros, E. González, P. Mira, Revue française de génie civil **6** (6), 1213 (2002).

2. V. Vilímek, J. Klimeš, J. Vlcko, R. Carreño, Environmental Geology **50** (7), 1041 (2006).

3. A. C. Tillery, M. J. Darr, S. H. Cannon, J. A. Michael, US Geological Survey Open-File Report **1257** (9) (2011).

4. L. Fan, P. Lehmann, B. McArdell, D. Or, Geomorphology **280**, 1 (2017).

5. E. T. Selig, J. M. Waters, *Track geotechnology and substructure management*. (1994).

6. E. T. Selig, presented at the Proceedings 6th International Heavy Haul Railway Conference, Cape Town, South Africa, 1997 (unpublished).

7. K. Rushton, G. Ghataora, presented at the Proceedings of the Institution of Civil Engineers-Transport, 2009 (unpublished).

8. N. Tennakoon, B. Indraratna, C. Rujikiatkamjorn, S. Nimbalkar, T. Neville, Geotechnical Testing Journal **35** (4), 629 (2012).

9. J. I. Shu, Y. Wang, Y. Qian, J. A. Khan, S. R. Schmidt, Transportation Geotechnics **28**, 100532 (2021).

10. Y. Gong, Y. Qian, X. Chen, Transportation Research Record **0** (0), 03611981221098659 (2022).

11. J. Zhao, T. Shan, Powder Technology **239**, 248 (2013).

12. L. Jing, C. Kwok, Y. Leung, Z. Zhang, L. Dai, Journal of Geophysical Research: Earth Surface **123** (8), 2004 (2018).

13. X. He, H. Xu, W. Li, D. Sheng, Computers and Geotechnics **128**, 103818 (2020).

14. Y. Qian, S. Zhu, Y. Wang, D. C. Rizos, presented at the ASME/IEEE Joint Rail Conference, 2018

15. G. Cui, M. Liu, W. Dai, Y. Gan, International Journal of Multiphase Flow **114**, 19 (2019).

16. C. T. Crowe, J. D. Schwarzkopf, M. Sommerfeld, Y. Tsuji, *Multiphase flows with droplets and particles*. (CRC press, 2011).

Fig. 2. Illustration for the local fouling occupancy (LFO)